Performance Characteristics of a High-Sensitivity, Three-Wavelength, Total Scatter/Backscatter Nephelometer

T. L. ANDERSON,* D. S. COVERT,* S. F. MARSHALL,*† M. L. LAUCKS,* R. J. CHARLSON,* A. P. WAGGONER,*# J. A. OGREN,@ R. CALDOW,& R. L. HOLM,& F. R. QUANT,& G. J. SEM,& A. WIEDENSOHLER,** N. A. AHLQUIST,†† AND T. S. BATES##

*Department of Atmospheric Sciences, University of Washington, Seattle, Washington
@NOAA/Climate Monitoring and Diagnostics Laboratory, Boulder, Colorado
&TSI Incorporated, St. Paul, Minnesota
**Institut für Troposphärenforschung e. V., Leipzig, Germany
††FloScan Instrument Company, Incorporated, Seattle, Washington
##NOAA/Pacific Marine Environmental Laboratory, Seattle, Washington

(Manuscript received 18 November 1995, in final form 15 March 1996)

ABSTRACT

As designed in the 1940s by Beuttell and Brewer, the integrating nephelometer offers a direct method of measuring light scattering by airborne particles without assumptions about particle composition, shape, or physical state. A large number of such instruments have been deployed; however, only a limited number of validation experiments have been attempted. This paper reports a set of *closure* experiments in which a gas-calibrated nephelometer is used to measure the scattering coefficient of laboratory-generated particles of known size and refractive index.

Specifically, it evaluates the performance of a high-sensitivity, three-wavelength, total scatter/backscatter integrating nephelometer (TSI, Inc., model 3563). Sources of uncertainty associated with the gas-calibration procedure, with photon-counting statistics, and with nonidealities in wavelength and angular sensitivity are investigated. Tests with particle-free gases indicate that noise levels are well predicted by photon-counting statistics and that the nephelometer response is linear over a wide range of scattering coefficients. Tests with particles show average discrepancies between measured and predicted scattering of 4%–7%. Error analysis indicates that these discrepancies are within experimental uncertainty, which was dominated by particle generation uncertainty. The simulation of nephelometer response, which is validated by these tests, is used to show that errors arising from nephelometer nonidealities are less than 10% for accumulation-mode or smaller particles (i.e., size distributions for which the volume mean diameter is 0.4 μm or less) and that significant differences exist between the total scatter and backscatter uncertainties. Based on these findings, appropriate applications of the model 3563 nephelometer are discussed.

1. Introduction

The attenuation of parallel beam light during its passage through an absorbing and/or scattering medium is described by the Beer–Lambert law [see Eq. (A1)] in which the space rate of attenuation is called the extinction coefficient σ_{ext} with units of inverse distance. In the atmosphere, the extinction coefficient is conveniently separated into four components: absorption by gas molecules σ_{ag}, scattering by gas molecules σ_{sg}, absorption by particles σ_{ap}, and scattering by particles σ_{sp}, each of which is a function of wavelength. For solar wavelengths, light scattering by atmospheric aerosol particles σ_{sp} is the dominant component of extinction near the earth's surface and in the column integral for clear sky conditions. Thus, σ_{sp} is an important factor in both visibility and climate change research. The purpose of an integrating nephelometer is to provide a direct measurement of σ_{sp} (and a companion quantity σ_{bsp} defined below) that is independent of the size, composition, and physical state of the light-scattering particles. This article evaluates the performance of a specific nephelometer in relation to that purpose.

As devised by Beuttell and Brewer (1949), the integrating nephelometer performs a geometrical integration (see the appendix) of the angular distribution of scattered intensity such that the scattering coefficient of a gaseous or aerosol medium can be measured with the combination of a Lambertian light source and an orthogonal light detector. The enclosed version

†Current affiliation: PRC, Incorporated, Reston, Virginia.
#Current affiliation: Boeing Corporation, Seattle, Washington.

Corresponding author address: Dr. T. L. Anderson, Department of Atmospheric Sciences, University of Washington, Box 351640, Seattle, WA 98195-1640.
E-mail: tadand@atmos.washington.edu

(Ahlquist and Charlson 1967) allows calibration with gases of known scattering coefficient. Scattering by particle-free air can be measured and subtracted from subsequent measurements on an aerosol to derive σ_{sp}. The addition of a shutter that blocks illumination from the region corresponding to scattering angles less than 90° (Charlson et al. 1974) allows measurement of the hemispheric backscattering coefficient due to aerosol particles, a quantity that we will designate σ_{bsp}. A high-sensitivity, photon-counting version first reported by Heintzenberg and Bäcklin (1983) incorporates 1) a rotating shutter to correct for dark count, changes in lamp brightness, and changes in photomultiplier tube sensitivity, and 2) continuous temperature and pressure measurements within the sensing volume for adjusting the value of air scattering used to derive particle scattering. These features plus beam splitters for simultaneous measurement at three wavelengths are described in detail by Bodhaine et al. (1991). In this paper we investigate a commercially produced nephelometer (TSI, Inc., model 3563) that combines the closed geometry of Ahlquist and Charlson (1967) with the high-sensitivity, multiwavelength features presented by Bodhaine et al. (1991), as well as a backscatter shutter.

Practical design limitations impose nonidealities on the wavelength and angular sensitivities of any nephelometer. Nonidealities in wavelength sensitivity arise because scattering is measured over a narrow but finite wavelength range that is not perfectly centered on the nominal wavelength. Nonidealities in angular sensitivity arise because 1) illumination intensity should be cosine-weighted but is not perfectly so, 2) the nephelometer geometry restricts the photomultiplier tubes to viewing scattering angles from about 7° to 170°, and 3) light blockage by the backscatter shutter does not provide a perfectly sharp separation at 90°. Rayleigh scattering (e.g., visible light scattered by gas molecules and particles with diameters D_p less than about 50 nm) is characterized by simple dependencies such as σ_{sp} proportional to D_p^6 and equal scattering in the backward and forward hemispheres. In this scattering regime, nephelometer nonidealities have a constant (non-size-dependent) effect; therefore, the nephelometer measures with an accuracy limited only by the accuracy of the gas calibration and photon-counting statistics. However, it is the Mie scattering regime (50 nm $< D_p <$ 5 μm for visible light) that is generally of interest in nephelometer applications because this is where most particle mass exists and where particles scatter light most efficiently. In this regime, the scattering phase function varies strongly with size; therefore, nephelometer nonidealities introduce particle-size-dependent errors that constitute an additional source of uncertainty (Ensor and Waggoner 1970; Heintzenberg and Bhardwaja 1976; Heintzenberg 1978).

The purpose of this article is to quantify these nephelometer uncertainties, including their particle-size dependence, for the TSI model 3563. To achieve this, a series of laboratory experiments were made using 1) gases at constant density to study noise levels, 2) gases of varying density and refractive index to study linearity of response, and 3) monodisperse particles of known size and refractive index to study response in the Mie scattering regime. Results of the noise studies are compared to predictions based on Poisson statistics of photon counting. Results of the particle tests are compared to Mie simulations using the measured wavelength and angular sensitivities of the model 3563.

2. Methods

a. *Definition of scattering quantities related to nephelometer measurements*

The TSI 3563 integrating nephelometer (Fig. 1) is designed to measure six *extensive*[1] quantities: $\sigma_{sp}^{\lambda_i}$ and $\sigma_{bsp}^{\lambda_i}$, the scattering coefficient and backscattering coefficient, respectively, by aerosol particles for monochromatic radiation at each of three wavelengths, λ_i (450, 550, and 700 nm; also referred to herein as "blue," "green," and "red"). From these measurements, *intensive* optical properties related to the phase function and wavelength dependence of scattered light can be derived. The nephelometer signals (photon counts) provide a relative measure of the scattering coefficient, such that $\sigma_{sp}^{\lambda_i}$ and $\sigma_{bsp}^{\lambda_i}$ can be derived only after the nephelometer has been calibrated with gases of known low and high scattering coefficients. The low span gas is normally air, although other gases or even a vacuum can also be used. This calibration procedure determines the slope K_2 and offset W of a calibration line as depicted in Fig. 2. The offset W may be physically interpreted as photon counts due to scattering by internal surfaces (wall scatter). In the following sections, the uncertainties in nephelometer measurements stemming from the gas calibration will be defined and estimated.

Results of our calibration studies with particles are most readily interpreted by distinguishing four quantities related to the scattering coefficient. Letting σ represent any of the six scattering coefficients measured by the nephelometer (that is, dropping the sub-superscripts $_{sp}^{\lambda_i}$ and $_{bsp}^{\lambda_i}$ for clarity), these four quantities will be designated as σ_k (for "known"), σ_m (for "measured"), σ_{sim} (for "simulated"), and σ_p (for "predicted"). Here σ_k is the actual scattering coefficient that would be measured by an ideal nephelometer (see the appendix) or as predicted by Mie theory (assuming, as is the case in our experiments, that the particles are internally homogeneous spheres). The scattering coefficient as measured by a gas-calibrated nephelometer

[1] With regard to atmospheric aerosol properties, an *extensive* quantity is a function of the amount of particulate matter present per unit volume whereas an *intensive* quantity is not.

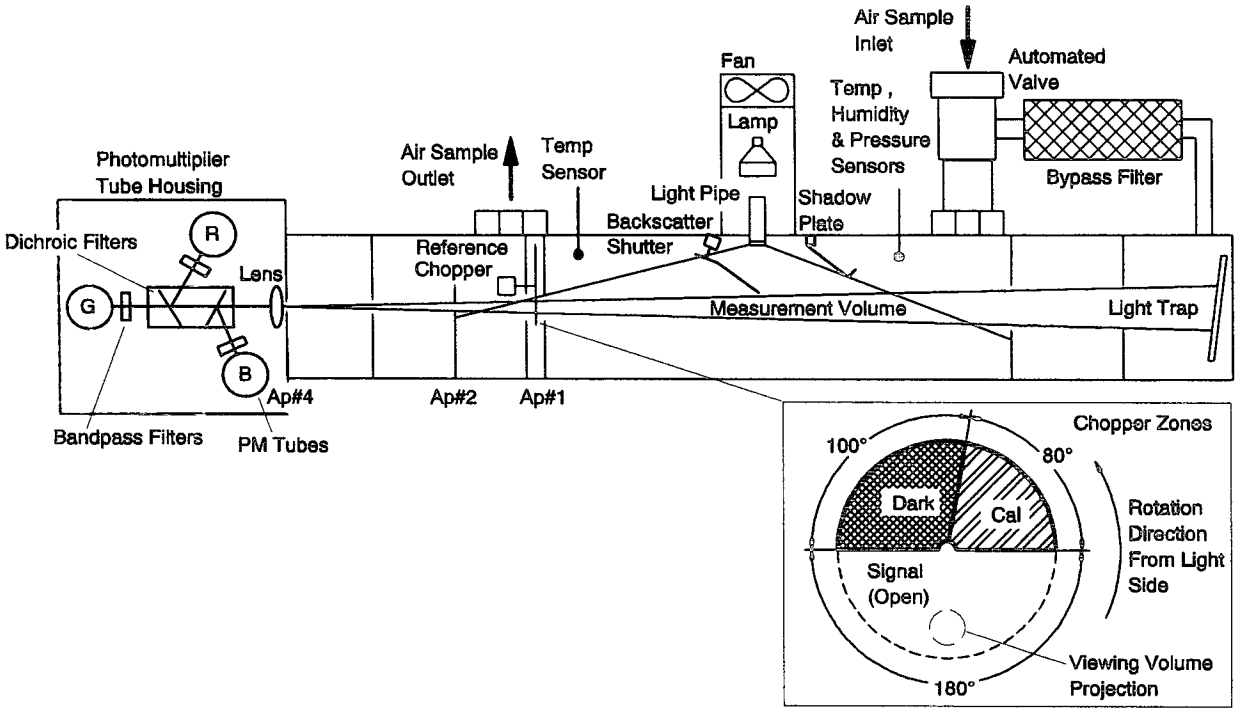

FIG. 1. Design features of the TSI 3563 integrating nephelometer. The main body consists of a 10-cm-diameter, thin-walled aluminum tube approximately 90 cm long. Receiving optics are located at one end of the tube with a light trap at the other end to provide a very dark background against which to view the light scattered by particles and gases. Illumination is provided by a 75-W quartz-halogen lamp, with a built-in elliptical reflector. The reflector focuses the light onto one end of an optical pipe, which serves to thermally isolate the lamp from the sensing volume. The output end of the optical pipe is an opal glass diffuser that provides a nearly Lambertian light source. Within the measuring volume, the first aperture on the detection side (Ap#1) limits the light integration to angles greater than about 7°, measured from the horizontal surface of the opal glass. On the other side, a shadow plate limits the integration to angles less than about 170°. The measurement volume is defined by the intersection of illumination light with a conical viewing volume established by the second and fourth aperture plates. The fourth aperture plate incorporates a lens to collimate the scattered light so that it can be split into separate wavelengths by means of dichroic and bandpass filters. Detection at each wavelength is by photomultiplier tubes (PMT). The reference chopper, which rotates at 23 Hz, consists of three separate areas—signal, dark, and calibrate—as shown in the inset. The signal section simply allows all light to pass through unaltered. The dark section blocks all light to provide a measurement of PMT background noise. The calibrate section scatters a small fraction of illumination light directly to the PMTs to provide a measure of lamp stability over time. To subtract the light scattered by internal surfaces and the gas portion of the aerosol, a bypass filter (high-efficiency HEPA) is switched periodically in line with the inlet. Correction for changes in gas density is accomplished continuously by means of pressure and temperature sensors. In addition, the relative humidity of the sample volume is monitored, and a second temperature sensor at the outlet keeps track of sample heating. A rotating backscatter shutter periodically cuts off illumination at 90° allowing hemispheric backscattering (angles from 90° to 170°) to be measured as well as total scattering (angles from 7° to 170°).

is σ_m; σ_{sim} is the scattering coefficient calculated by Mie theory but integrated over the measured wavelength and angular sensitivities of the nephelometer. Note that σ_{sim} represents the scattering integral actually sensed by the nephelometer but does not take into account the gas calibration. When σ_{sim} is multiplied by a correction factor K_R, which accounts for the gas calibration, we have σ_p, the predicted nephelometer measurement.

In its simplest form, the linear equation relating nephelometer photon counts C to the measured scattering coefficient σ_m is

$$\sigma_m = K_2 C - W, \qquad (1)$$

where the slope K_2 and offset W are determined by calibration with two span gases (typically air and CO_2) as shown in Fig. 2. In essence, the gas calibration sets the constants K_2 and W such that

$$\sigma_{m-R} = \sigma_{k-R} = K_R \sigma_{sim-R}, \qquad (2)$$

where the subscript R denotes Rayleigh regime.

Equation (2) indicates that a secondary effect of the gas calibration is to correct for nephelometer nonidealities. If the actual wavelength and angular sensitivities [$f(\lambda)$ and $f(\theta)$, respectively] are measured and used as input to a modified Mie integration (Fig. 3a), a correction factor K_R can be estimated that expresses the ratio of σ_k to the scattering integral actually sensed by the nephelometer σ_{sim}. Because the angular distribution of scattered intensity does not change with particle size or wavelength in the Rayleigh regime, K_R is a constant

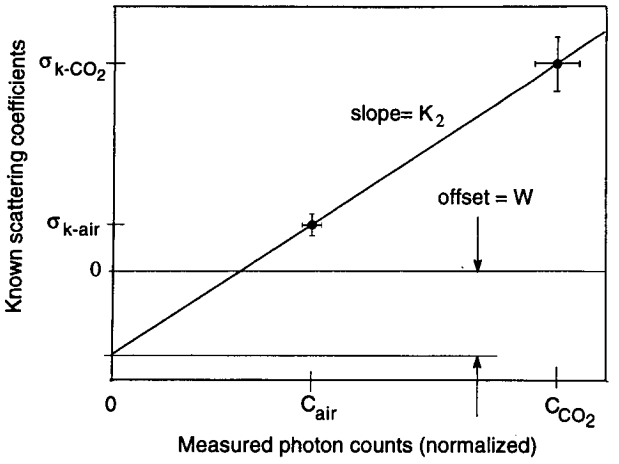

FIG. 2. Calibration of the nephelometer is based on the assumption of a linear response to changing scattering coefficient. The slope of the calibration line K_2 is determined by measuring the normalized photon-counting rates C associated with high and low span gases of known scattering coefficient σ_k. Standard dry air and CO_2 were used in our experiments, as depicted above. The zero offset W could be determined by extrapolating this line to a photon-counting rate of zero. In practice, W is determined by a zeroing procedure (not depicted) in which filtered, particle-free air is introduced into the nephelometer.

and (2) holds, as indicated, not just for the calibration gases but for any Rayleigh scattering medium.

In the Mie regime, scattered intensity is a highly irregular function of scattering angle and this function is strongly dependent on particle size and wavelength. For homogeneous, spherical particles of known size and refractive index, a modified Mie integration (i.e., integration of the Mie phase function over the nephelometer angular and wavelength sensitivities) can still be used to calculate σ_{sim}, but the ratio between this quantity and σ_k will no longer be a constant. If such particles are introduced into a gas-calibrated nephelometer (as in our particle experiments), the nephelometer measurement as a function of particle diameter, $\sigma_m(D_p)$ can be compared to a predicted measurement $\sigma_p(D_p)$, which derives from the nephelometer simulation and the Rayleigh correction factor

$$\sigma_p(D_p) = K_R\sigma_{sim}(D_p). \quad (3)$$

The comparison of σ_p with σ_m constitutes a closure experiment (Fig. 3b), which can either succeed or fail to find agreement within the experimental uncertainties. In the latter case, measurements, assumptions, and calculations must be checked and the experiment repeated. Once a successful closure experiment has been achieved, the discrepancy between σ_p and σ_m provides an objective measure of the combined uncertainty of the theoretical and experimental methods. Furthermore, the nephelometer simulation can then be extrapolated to a broad range of sizes or size distributions to enable a general investigation of size-dependent performance characteristics. For this purpose, σ_p is compared to σ_k, the "known" or "true" scattering coefficient, as indicated in Fig. 3c.

b. Calibration equations

The TSI 3563 nephelometer converts photon counts to particle scattering coefficient σ_{sp} and backscattering coefficient σ_{bsp} as follows:

$$\sigma_{sp} = K_2C_m - W - \sigma_{k-air}(T, P) \quad (4)$$

$$\sigma_{bsp} = K_2C_{mb} - W_b - K_4\sigma_{k-air}(T, P), \quad (5)$$

where K_2 (m^{-1}) is the calibration slope; W and W_b (m^{-1}) are the wall scatter constants for total scatter and backscatter, respectively; $\sigma_{k-air}(T, P)$ (m^{-1}) is the calculated, temperature- and pressure-dependent scattering coefficient of standard dry air[2]; C_m and C_{mb} are the normalized photon count rates for total scatter and backscatter, respectively (normalization corrects for dark count and lamp drift); and K_4 is a backscatter correction factor. Note that (5) assumes that the calibration slope K_2 is the same for backscatter as for total scatter, thereby allowing the additional correction factor K_4 to be introduced. This assumption is slightly unrealistic in that K_2 not only converts photon counts to scattering coefficient but also corrects for the angular sensitivities of the nephelometer, which may differ between backscatter and total scatter. That is, K_2 implicitly includes the Rayleigh-regime correction factor K_R discussed above [see Eqs. (2) and (3)]. The factor K_4 is determined by the calibration procedure and is intended to correct for cases where the backscatter shutter is slightly off center—as indicated by K_4 values that differ slightly from 0.5. According to this calibration procedure, the backscatter-to-total-scatter ratio for gases or Rayleigh-regime particles is set to K_4, whereas the target value of this ratio (90°–180° backscatter divided by 0°–180° total scatter) is 0.5. An alternate calibration procedure would be to replace K_2 in (5) with a separate backscatter calibration slope K_{2b}, and replace K_4 with a constant value of 0.5. However, the two methods are nearly identical as long as K_4 comes out within a few percent of 0.5.

Calibration is accomplished by introducing particle-free span gases of known scattering coefficient into the nephelometer and solving the following four equations for calibration constants K_2, K_4, W, and W_b:

low span gas:

$$\sigma_{sp} = K_2C_{lo} - W - \sigma_{k-lo} = 0 \quad (6)$$

$$\sigma_{bsp} = K_2C_{lob} - W_b - K_4\sigma_{k-lo} = 0 \quad (7)$$

[2] Standard dry air is defined as 78.09% N_2, 20.95% O_2, 0.93% Ar, and 0.03% CO_2 by volume.

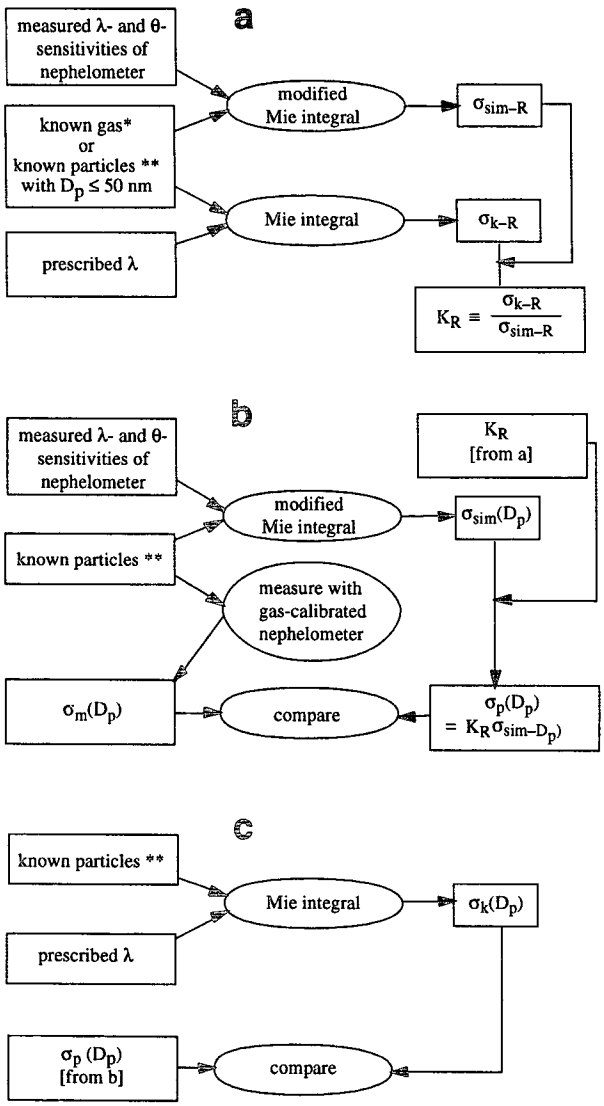

* scattering coefficient is known as a function of wavelength, temperature, and pressure.

**spherical, internally homogeneous particles of known size (or known size distribution), refractive index, and concentration per volume of air.

FIG. 3. Conceptual depiction of nephelometer characterization experiments; λ refers to wavelength and θ to scattering angle. The subscript R refers to Rayleigh-regime scattering; D_p indicates particle diameter; σ_k, σ_m, σ_{sim}, and σ_p are the known, measured, simulated, and predicted scattering coefficients, respectively.

high span gas:

$$\sigma_{sp} = K_2 C_{hi} - W - \sigma_{k-hi} = 0 \tag{8}$$

$$\sigma_{bsp} = K_2 C_{hib} - W_b - K_4\sigma_{k-hi} = 0, \tag{9}$$

where the C's and σ_k's are normalized photon count rates and known scattering coefficients, respectively, as before. The solutions for K_2 and K_4 are

$$K_2 = \frac{\sigma_{k-hi} - \sigma_{k-lo}}{C_{hi} - C_{lo}} \tag{10}$$

$$K_4 = \frac{C_{hib} - C_{lob}}{C_{hi} - C_{lo}}. \tag{11}$$

Wall scatter values W and W_b can be determined and adjusted between calibrations by a zeroing procedure in which filtered air is introduced into the nephelometer. Their values are given by

$$W = K_2 C_z - \sigma_{k-z} \tag{12}$$

$$W_b = K_2 C_{zb} - K_4\sigma_{k-z}, \tag{13}$$

where the subscript z denotes photon counts or scattering coefficients associated with the filtered, "zero" air. Automated and routine zeroing with ambient air not only corrects for changes in scattering by internal wall surfaces but also corrects for changes in refractive index of the carrier gas due, for instance, to changes in water vapor content. Thus, while the calibration slope K_2 is best determined with tank gases for which the scattering coefficients are most accurately known, the calibration offsets W and W_b are best determined with filtered ambient air under normal sampling conditions.

c. *Measurement uncertainties*

1) GENERAL UNCERTAINTY EQUATION

If quantity y depends on parameters p_i, the uncertainty of each parameter contributes to y uncertainty according to the derivative of y with respect to that quantity. These contributions sum in quadrature. Designating uncertainties with the prefix δ and derivatives with the prefix ∂, we have

$$\delta y^2 = \sum_i \left(\frac{\partial y}{\partial p_i}\,\delta p_i\right)^2, \tag{14}$$

where we have assumed independent parameters p_i, such that correlation terms can be neglected. The nephelometer measurements can be expressed in terms of basic, independent parameters by substituting (10) through (13) into (4) and (5), respectively, to give

$$\sigma_{sp} = \frac{\sigma_{k-hi} - \sigma_{k-lo}}{C_{hi} - C_{lo}}(C_m - C_z) - (\sigma_{k-air} - \sigma_{k-z}) \tag{15}$$

$$\sigma_{bsp} = \frac{\sigma_{k-hi} - \sigma_{k-lo}}{C_{hi} - C_{lo}}(C_{mb} - C_{zb}) - \frac{C_{hib} - C_{lob}}{C_{hi} - C_{lo}}(\sigma_{k-air} - \sigma_{k-z}). \tag{16}$$

Equations (15) and (16) show that the basic parameters underlying the nephelometer measurements are all dif-

ferences. These differences divide into two categories: those involving photon counts C, and those involving known gas scattering coefficients σ_k. If the carrier gas and zero gas are the same, all terms involving the difference $(\sigma_{k-\text{air}} - \sigma_{k-z})$ drop out, such that the calibration and photon-counting uncertainties are given by

$$(\delta\sigma_{sp})^2 = \underbrace{\left[\frac{\sigma_{k-\text{hi}} - \sigma_{k-\text{lo}}}{C_{\text{hi}} - C_{\text{lo}}}\,\delta(C_m - C_z)\right]^2}_{\text{meas. and zero count (noise)}} + \underbrace{\left[\frac{(\sigma_{k-\text{hi}} - \sigma_{k-\text{lo}})(C_m - C_z)}{(C_{\text{hi}} - C_{\text{lo}})^2}\,\delta(C_{\text{hi}} - C_{\text{lo}})\right]^2}_{\text{calibration count}} + \underbrace{\left[\frac{C_m - C_z}{C_{\text{hi}} - C_{\text{lo}}}\,\delta(\sigma_{k-\text{hi}} - \sigma_{k-\text{lo}})\right]^2}_{\text{calibration gases}}. \quad (17)$$

The uncertainty equation for backscatter σ_{bsp} is identical to (17) except that C_m and C_z are replaced with C_{mb} and C_{zb}, respectively. Equation (17) identifies three sources of nephelometer uncertainty: uncertainty of photon counts during the measurement and zeroing procedures, uncertainty of photon counts during the calibration, and uncertainty in the scattering coefficients of the calibration gases. In eliminating the term containing $\delta(\sigma_{k-\text{air}} - \sigma_{k-z})$, we have implicitly assumed that carrier- and zero-gas uncertainties are systematic (not random). This point is further explained and justified below.

2) CALIBRATION GAS UNCERTAINTIES

The scattering coefficient of a gas varies with temperature T and pressure P according to the ideal gas law

$$\sigma_{k-\text{gas}} = \sigma_{k-\text{gas}}(\text{STP})\left(\frac{273.2}{T}\right)\left(\frac{P}{1013.2}\right), \quad (18)$$

where standard temperature and pressure (STP) has been defined as 273.2 K and 1013.2 mb. Equation (18) implies that σ_k uncertainties can be separated into two components:

$$(\delta\sigma_{k-\text{gas}})^2 = [\delta\sigma_{k-\text{gas}}(\text{STP})]^2 + [\delta\sigma_{k-\text{gas}}(\text{env})]^2, \quad (19)$$

where $\delta\sigma_{k-\text{gas}}(\text{STP})$ refers to uncertainty in the literature-derived values of scattering coefficient at STP, and $\delta\sigma_{k-\text{gas}}(\text{env})$ refers to gas density uncertainties in the nephelometer sensing environment. To evaluate the former term, we first introduce the standard equation (e.g., see Middleton 1952, p. 19) for the scattering coefficient of a gas:

$$\sigma_{k-\text{gas}}(\text{STP}, \lambda) = \frac{8\pi^3}{3}\frac{(n^2 - 1)^2}{N_0\lambda^4}F_K, \quad (20)$$

where n is the refractive index of the gas at wavelength λ, N_0 is the molecular number density at STP (2.687E25 molecules per cubic meter), and F_K is the depolarization factor (King 1923) that accounts for additional scattering by optically anisotropic molecules compared to isotropic molecules of the same refractive index. Standard formulas for refractive index of air and CO_2 (CRC 1994, 10–302; Owens 1967; Eldén 1966) give $(n - 1)$ to an accuracy of better than four significant figures, which translates into σ_k uncertainties of less than 0.1%. The depolarization factors are a more significant source of uncertainty. For air, the best available data indicate F_K values of 1.050, 1.049, and 1.048 for the respective nephelometer wavelengths of 450, 550, and 700 nm (Bucholtz 1995) with an uncertainty of about ±0.0025 (Young 1980). For CO_2, F_K values of 1.156, 1.153, and 1.149 for the same three wavelengths and an uncertainty of ±0.0104 for all wavelengths have been adopted based on wavelength-dependent measurements by Alms et al. (1975) and the range of values reported by various investigators (Penndorf 1957; Cutten 1974; Alms et al. 1975; Young 1980). The central values recommended here are slightly smaller than those based on Penndorf (1957), which were adopted in a previous determination of σ_k values for use in nephelometer calibrations (Bodhaine et al. 1991). Table 1 summarizes the recommended values and uncertainties of $\sigma_k(\text{STP}, \lambda)$ for air and CO_2. These values are consistent with a CO_2-to-air scattering ratio of 2.59 ± 0.03, which can be compared to 2.61 ± 0.03 measured by Bhardwaja (1973) with an air-He calibrated nephelometer and to a ratio of 2.59 determined theoretically by Cutten (1974).

The absolute accuracy of the T and P measurements within the nephelometer are given by the manufacturer as $\delta T = \pm 0.5$ K and $\delta P = \pm 1.5$ mb. For temperature, there is an additional source of uncertainty arising from the heating of the airstream by the lamp. This causes a small temperature gradient within the nephelometer sens-

TABLE 1. Recommended values* and uncertainties of scattering coefficients for air and CO_2.

Wavelength (nm)	δ_{k-air}(STP) (Mm^{-1})		$\delta\sigma_{k-air}$(STP) (Mm^{-1})	σ_{k-CO_2}(STP) (Mm^{-1})		$\delta\sigma_{k-CO_2}$(STP) (Mm^{-1})
	B91**	This work	This work	B91	This work	This work
450	27.89	27.61	±0.24%	72.79	71.83	±0.90%
550	12.26	12.125	±0.24%	31.99	31.40	±0.90%
700	4.605	4.549	±0.24%	12.01	11.74	±0.90%

* Values given at STP (273.2 K and 1013.2 mb) and for each of the nominal nephelometer wavelengths.
** B91 refers to values recommended by Bodhaine et al. (1991).

ing volume and thus some uncertainty as to the appropriate average temperature. We will assume this uncertainty is 0.2 times the difference between inlet and outlet temperatures, which was 4 K for our tests. The total temperature uncertainty is thus given by the square root of $(0.5^2 + 0.8^2)$—that is, $\delta T = \pm 0.9$ K. Applying (14) to (18), we can evaluate the relative uncertainty in σ_k due to gas density uncertainties near sea level as

$$\left[\frac{\delta\sigma_{k-gas}(env)}{\sigma_{k-gas}}\right]^2 = \left(\frac{\Delta T}{T}\right)^2 + \left(\frac{\Delta P}{P}\right)^2 = (0.31\%)^2 + (0.15\%)^2 = (0.34\%)^2. \quad (21)$$

Using this value and those in Table 1, the total relative uncertainties in σ_k are about 0.42% for air and 0.95% for CO_2.

3) EFFECTS OF WATER VAPOR

So far we have assumed that "air" is always standard dry air. The effect on scattering coefficient for different molecular mixtures is a function of the changes in refractive index and depolarization factor. From (20) we have

$$\frac{\sigma_{k-mix}}{\sigma_{k-std}} = \frac{(n^2_{mix} - 1)^2}{(n^2_{std} - 1)^2}\frac{F_{K-mix}}{F_{K-std}}, \quad (22)$$

where σ_{k-std} refers to standard dry air and σ_{k-mix} refers to air with a different molecular composition. Refractive index effects were studied by Owens (1967). His results indicate that for all reasonable sampling conditions (e.g., as long as direct sampling of smoke stacks is avoided), the only significant deviations from standard dry air come about from the presence of water vapor.

The effect of water vapor on scattering coefficient is proportional, to an excellent approximation, to the fraction of water molecules in the gas, e/P (where e and P are the water vapor pressure and total pressure, respectively). Thus, we can introduce a water vapor correction factor η, which accounts for both the refractive index and depolarization effects,

$$\frac{\sigma_{k-wet}}{\sigma_{k-dry}} = 1 - \eta\frac{e}{P} = 1 - \eta\frac{e_s(T)}{P}\frac{RH}{100}. \quad (23)$$

Here $e_s(T)$ is the saturation water vapor pressure at temperature T. The results of Owens (1967) indicate that $\eta = 0.31$; however, this assumes that water vapor and standard dry air have the same depolarization factor (about 1.05). We were unable to find literature values for F_{K-H_2O}. Since the electron cloud surrounding a water molecule is more nearly spherical than for either O_2 or N_2, F_{K-H_2O} is probably less than 1.05. As limiting cases, we assume $1.00 < F_{K-H_2O} < 1.10$, which yields $\eta = 0.31 \pm 0.05$. At 30°C, $e_s(T) = 42.4$ mb. For this temperature, therefore, assuming $P = 1013.2$ mb, an RH of 30% would change σ_{k-air} by $-0.39\% \pm 0.06\%$ compared to dry air, while an RH of 85% would change σ_{k-air} by $-1.1\% \pm 0.2\%$. For a given value of RH, this effect diminishes rapidly at lower temperatures and increases rapidly at higher temperatures due to the strong nonlinearity of the function $e_s(T)$.

There are two sources of error associated with this water vapor effect. During calibration it could result in slightly erroneous values of σ_{k-lo}, which would affect K_2. This possibility can be eliminated by using dry air (bottled standard air or dried ambient air) during calibrations. During measurements and zeroing procedures the presence of water vapor could result in slightly erroneous values of σ_{k-air} and σ_{k-z}. However, as shown in (15) and (16), these errors would offset each other as long as the vapor pressure within the nephelometer does not change. [For humidity-controlled, RH-scanning nephelometers (Covert et al. 1972) this is clearly a poor assumption.] Thus, a useful protocol is to calibrate with dry air and perform zeroing procedures with ambient air. If such a procedure is adopted, as it was in these experiments, water vapor errors become negligible. If dry air is not available, a correction factor for σ_{k-lo} can be calculated from (23) and the measured T and RH in the nephelometer.

4) PHOTON-COUNTING UNCERTAINTIES

Photon-counting uncertainties affect both measurement noise and accuracy, the latter arising from uncer-

tainties during calibration. Both these sources of uncertainty can be estimated from the reported photon count rates and Poisson statistics. Photon counts exist in three forms—raw, scaled, and normalized. Raw counts C_{raw} and scaled count rates C_s (in hertz) are defined for the three portions of the rotating shutter (see Fig. 1 inset)—calibrate, signal, and dark. The normalized photon counts C presented in (15) through (17) above, combine the three scaled counts to derive a signal that is corrected for dark counts and changes in lamp brightness:

$$C = \frac{C_{s-\text{sig}} - C_{s-\text{dark}}}{C_{s-\text{cal}} - C_{s-\text{dark}}}. \tag{24}$$

The conversion from raw to scaled counts is given in each case by

$$C_s = 2\frac{C_{\text{raw}}}{\tau}\frac{360^\circ}{G}, \tag{25}$$

where τ is the sample time and G is the gate width (in degrees) for the appropriate portion of the rotating shutter—40° for calibrate, 140° for signal, and 60° for dark. The factor of 2 arises because half the time is spent counting backscatter photons; however, this factor is omitted for dark counts that are accumulated during both positions of the backscatter shutter. (A small correction for photomultiplier dead time, which does not affect the uncertainty analysis because it only comes into play at very high photon count rates, is neglected in this discussion.)

The Poisson uncertainty for raw photon counts is

$$\delta C_{\text{raw}} = C_{\text{raw}}^{1/2}. \tag{26}$$

Thus, the uncertainty for each of the three types of scaled counts is given by

$$\delta C_s^2 = \frac{2 \times 360 \times C_s}{\tau G}. \tag{27}$$

The uncertainty of the normalized photon counts C will be, according to (14)

$$\delta C^2 = \sum_j \left(\frac{\partial C}{\partial C_{s-j}}\delta C_{s-j}\right)^2, \tag{28}$$

where the index j refers to the three types of scaled counts—signal, calibrate, and dark—shown in (24) and C can refer to any of the normalized count rates indicated in (17).

5) Summed uncertainties due to noise and calibration

We are now in a position to evaluate each of the terms in (17) and its equivalent for backscatter. For the σ_k parameters, uncertainties are given in Table 1 and (21). For the C parameters (normalized photon-counting rates), (28) can be applied given the averaging time and the scaled photon-counting rates as reported by the nephelometer. The summed uncertainty applies to an ideal nephelometer (see the appendix) and/or to any Rayleigh-scattering medium (where nephelometer nonidealities do not come into play). It does not represent total nephelometer uncertainty in the Mie regime, since wavelength and angular nonidealities have not yet been considered [see section 2c(6)].

Note that uncertainty in the carrier gas scattering coefficient $\delta\sigma_{k-\text{air}}$ does not appear in (17). This term can be omitted if it can be assumed to be systematic for all measurements because the nephelometer is zeroed with the carrier gas. In that case, as shown in (15) and (16), systematic errors in $\sigma_{k-\text{air}}$ will be canceled out by identical errors in σ_{k-z}. Here $\delta\sigma_{k-\text{air}}$ arises from uncertainty in the literature values of $\sigma_{k-\text{air}}(\text{STP})$—which is obviously systematic—and from uncertainty in the gas density within the nephelometer. Thus, assuming that $\delta\sigma_{k-\text{air}}$ is systematic is equivalent to assuming that δT and δP are systematic—that is, that uncertainties in nephelometer temperature and pressure measurements have negligible contributions from random noise. This assumption is borne out by the absence of detectable variation of T and P during steady conditions and by the finding (presented in section 3a) that σ_{sp} and σ_{bsp} noise is well predicted by photon-counting uncertainties alone.

6) Wavelength and angular nonidealities

An ideal nephelometer (appendix) responds to monochromatic radiation emitted from a Lambertian, point source, and scattered by volume elements that act as point sources of scattered light. If, in addition, the sensing volume is infinitely long such that scattering angles from 0° to 180° are detected and the backscatter shutter performs a perfectly sharp cutoff at 90° of the illumination light, the signals of this nephelometer will be proportional to $\sigma_{sp}^{\lambda_i}$ and $\sigma_{bsp}^{\lambda_i}$, respectively. To evaluate the most important ways in which practical nephelometer designs differ from this ideal, we introduce a wavelength sensitivity function $f_i(\lambda)$ for each nominal wavelength λ_i and angular sensitivity functions for total scatter and backscatter, $f(\theta)$ and $f_b(\theta)$, respectively. These are defined such that

$$\int_0^\infty f_i(\lambda)d\lambda = 1 \tag{29}$$

$$\int_0^\pi f(\theta)d\theta = \int_0^\pi \sin\theta d\theta = 2 \tag{30}$$

$$\int_0^\pi f_b(\theta)d\theta = \int_{\pi/2}^\pi \sin\theta d\theta = 1. \tag{31}$$

To measure $f_i(\lambda)$, the light trap was removed and the detectors (40-nm bandwidth filters plus photomultiplier tubes) were directly illuminated with light from

a Beckman model B spectrophotometer. Wavelength-dependent response was scanned using approximately 2-nm increments. The resulting sensitivity functions (average plus/minus one standard deviation for four instruments) are plotted in Fig. 4a. For an ideal nephelometer, each $f_i(\lambda)$ would be a delta function centered at the nominal wavelength λ_i. Actual central wavelengths differ by 2–3 nm from these nominal values. This, plus the finite bandwidth, constitute a source of error in measurements of $\sigma_{sp}^{\lambda_i}$ and $\sigma_{bsp}^{\lambda_i}$ because the wavelength dependence of particle scattering varies with size and is different from that for the calibration gases.

We measured $f(\theta)$ and $f_b(\theta)$ in a manner similar to Heintzenberg (1978). The illumination system (halogen lamp, light pipe, opal glass, backscatter shutter, and shadow plate—Fig. 1) was placed on an optical bench and illumination intensity from 0° to 180° was measured with a goniometer. Results (again, average plus/minus one standard deviation for four instruments) are plotted in Fig. 4b. Low-angle truncation was measured geometrically from the mechanical design drawings.

For homogeneous, spherical particles of diameter D and complex refractive index m, Mie theory predicts the scattering intensity function $|S(\theta, X, m)|^2$ for scattering angle θ and size parameter X $(=\pi D\lambda^{-1})$. This can be integrated over angle to yield the single particle scattering efficiency (per unit cross-sectional area) Q:

$$Q_k(\lambda_i, m, D) = \frac{1}{X^2}\int_0^{\pi} |S(\theta, X, m)|^2 \sin\theta d\theta. \quad (32)$$

The subscript k is used in (32), following the discussion above, to indicate the "known" or "true" scattering value that the nephelometer is attempting to measure. To simulate the nephelometer response, a modified Mie integral is used in which $f(\theta)$ replaces $\sin(\theta)$ and integration over $f_i(\lambda)$ replaces the assumption of monochromatic light. Single particle scattering efficiency as sensed by the simulated nephelometer is designated Q_{sim}

$$Q_{\text{sim}}(\lambda_i, m, D) = \int_0^{\infty}\frac{1}{X^2}\int_0^{\pi} |S(\theta, X, m)|^2 f(\theta) d\theta f_i(\lambda) d\lambda. \quad (33)$$

Multiplication by particle cross-sectional area and integration over the particle size distribution, $N(D)$, yields the scattering coefficient sensed by the simulated nephelometer σ_{sim}.

$$\sigma_{\text{sim}}(\lambda_i, m, N(D)) = \int_0^{\infty} Q_{\text{sim}}(\lambda_i, m, D)\frac{\pi D^2}{4}\frac{\partial N}{\partial \log D} d\log D. \quad (34)$$

The nephelometer senses the scattering integral described by (33) and (34). However, it is calibrated with gases to report the correct scattering coefficient σ_k for any Rayleigh-scattering medium. To account for this calibration, we have introduced [Eq. (2); Fig. 3a] a Rayleigh-regime correction factor K_R. The predicted nephelometer measurement σ_p is given by the product of σ_{sim} and K_R, as shown in (3).

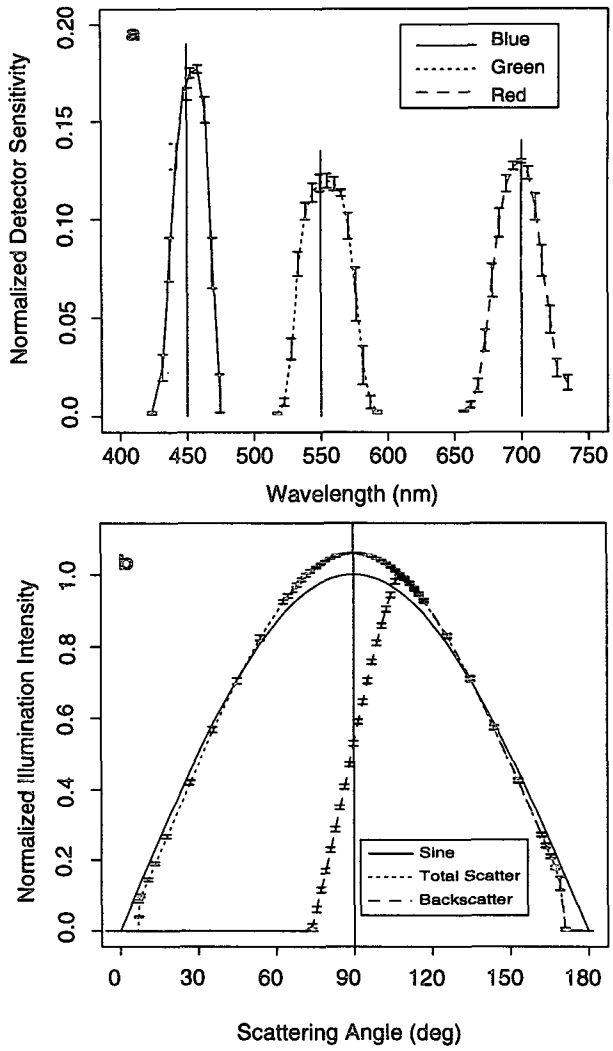

FIG. 4. Measured nephelometer nonidealities. Lines and error bars represent the average and plus/minus one standard deviation of measurements on four separate units. (a) Wavelength sensitivity [Eq. (29)]. The nominal wavelengths of 450, 550, and 700 nm are shown as vertical lines. (b) Angular sensitivity for total scatter [Eq. (30)] and backscatter [Eq. (31)] with the sine function shown for reference.

d. *Predicted scattering of laboratory generated particles*

For the particle tests, narrow size distributions of diethylhexyl-sebacate (DES) were produced with a condensation monodisperse aerosol generator (CMAG; model 3472, TSI, Inc.) and further narrowed by passage through a differential mobility analyzer (DMA;

model 3071A, TSI, Inc.) These two instruments are complementary in that the condensation process within the CMAG produces a small-particle tail that is eliminated by the DMA, while the potential for electrical mobility doublets and triplets from the bipolar charging process in the DMA is eliminated by the fact that the CMAG does not produce a tail at large sizes. Following the DMA, the aerosol stream was diluted and split, with 20 liters per minute (LPM) drawn through the nephelometer and 1 LPM drawn through a scanning mobility particle sizer (SMPS; model 3934, TSI, Inc.). The SMPS was used as a check for small or large particle tails and to estimate the breadth of the size distribution, which corresponded to a geometric standard deviation of less than 1.1 for all tests. Particulate number concentration was determined with a condensation particle counter (CPC; model 3010, TSI, Inc.) sampling directly from the nephelometer scattering volume. Flows for all instruments, but most critically for the DMA and CPC, were measured with an electronic bubble flow meter (Gilibrator, Sensidyne-Gilian Corp., Clearwater, Florida), with assumed uncertainty of ±1%.

The properties of DES are listed in Table 2. Information on the wavelength dependence of refractive index was obtained from the German CMAG manufacturer (Topas GmbH, Dresden, Germany). The stated uncertainty in refractive index (±0.005) is based on comparisons of the Topas GmbH data to our own measurements (1.450 ± 0.003 for white light) and to values listed (for 589.3 nm) in standard references (CRC 1994, 3–140; Merck 1989, p. 194, No. 1263). Use of bulk refractive index assumes the generated particles were pure DES; however, the CMAG requires nonvolatile "seed" particles to initiate condensation. In our case, these seed particles were 20-nm-diameter NaCl crystals, which introduce a maximum contamination of about 1 part per 1000 by volume. Since NaCl and DES have similar refractive indices (1.54 and 1.45, respectively) the presence of this NaCl contaminant is assumed to have a negligible affect on the particulate light scattering.

As a hydrophobic liquid, DES will form spherical particles, as assumed by Mie theory, which are unaffected by ambient water vapor. Light scattering by these particles can be predicted from a knowledge of refractive index, size distribution, and number concentration. (Light absorption is negligible.) The DMA produces a triangular size distribution, which we represent by central diameter D_{pc} and relative base width W, both of which can be predicted from the DMA flow and voltage settings. Thus, particle scattering is a function of four parameters: $\sigma_p(n, N, D_{pc}, W)$, where n is the real part of refractive index and N is number concentration (cm^{-3}). Refractive index uncertainties are given in Table 2. The uncertainty in N for particles well above the CPC detection limit is essentially identical to the flow-rate uncertainty of ±1%. For a 10:1 ratio of DMA sheath to sample flow as used in these experiments, W = 0.20 (full width at base of triangle relative to D_{pc}). We estimate the uncertainty of D_{pc} and W as ±2% and ±0.04, respectively, due to flow and geometrical uncertainties of the DMA (Kinney et al. 1991). Predicted scattering σ_p is calculated by the modified Mie integration described in (33) and (34). The uncertainty of this prediction is calculated by summing the uncertainties due to each of the four parameters—n, N, D_{pc}, and W—according to (14). This requires finding the derivative of σ_p with respect to each parameter. Here $\partial\sigma_p/\partial N$ is simply the average scattering per particle—a direct output of the modified Mie calculation. The other derivatives are found numerically using

$$\frac{\partial y}{\partial p_i} \approx \frac{y(p_i + \delta p_i) - y(p_i - \delta p_i)}{2\delta p_i}, \qquad (35)$$

where the parameter uncertainties δp_i are given above or in Table 2.

TABLE 2. Properties of di-ethylhexyl-sebacate (DES).

Alternate names:	decanedioic acid bis (2-ethylhexyl) ester; Bis (2-ethylhexyl) sebacate
Formula:	$C_{26}H_{50}O_4$
Molecular wt.:	426.7
Density (g cm^{-3}):	0.912 at 25°C
Refractive index:	1.456 ± 0.005 − 0.0i at 450 nm
	1.452 ± 0.005 − 0.0i at 550 nm
	1.446 ± 0.005 − 0.0i at 700 nm

3. Results

a. *Gas tests 1: Uncertainties due to calibration, zeroing, and noise*

Photon-counting rates for the high and low span gases are a useful diagnostic of nephelometer performance. From these data, which are reported by the model 3563 after each calibration, uncertainties for any averaging time and scattering level may be calculated using the formulas from the last section. Example data are given in Table 3. Based on these photon-counting rates, Table 4 presents detection limits, Fig. 5 and Table 5 present predicted photon-counting uncertainties in comparison to measured uncertainties, and Table 6 presents photon-counting uncertainties in comparison to other sources of uncertainty.

To measure nephelometer noise, tank air and CO_2 were sampled for one hour each and these data were grouped into 2-, 10-, 60-, and 300-s averages. Noise levels were assessed as the standard deviation for each grouping. These data showed no drift over time, so detrending was not necessary. Referring to (17), measurement noise levels involve random uncertainty in the quantity $(C_m - C_z)$. However, for measurements such as these based on a single zeroing procedure, C_z is constant such that measurement noise can be calculated from the Poisson uncertainty in C_m only. The compari-

TABLE 3. Typical nephelometer photon counts for air and CO_2.

	Scaled count rates (Hz)				Normalized count rates	
	$C_{S-\text{cal}}$	$C_{S-\text{dark}}$	$C_{S-\text{sig}}$	$C_{S-\text{sig}-b}$	C_{lo} or C_{hi}	$C_{\text{lo}b}$ or $C_{\text{hi}b}$
AIR (low-span gas)						
Blue	143 500	2	912	442	6.34E−03	3.07E−03
Green	437 000	4	1402	685	3.20E−03	1.56E−03
Red	527 200	207	1119	845	1.73E−03	1.21E−03
CO_2 (high-span gas)						
Blue	147 600	2	2303	1115	1.56E−02	7.54E−03
Green	446 300	3	3259	1601	7.30E−03	3.58E−03
Red	536 900	155	1881	1197	3.22E−03	1.94E−03

Scaled count rates as reported by the 3563 nephelometer for measurements made at 293 K and 950 mb. Quantities are defined in text surrounding Eqs. (24) and (25).

son between measured and calculated noise levels (Fig. 5) is quite good and does not indicate any systematic discrepancy. This implies that measurement noise is dominated by photon-counting uncertainty and can be predicted accurately from Poisson statistics. This further implies that random noise in the T and P measurements is not a significant source of uncertainty, which justifies our neglect of the term $\delta(\sigma_{k-\text{air}} - \sigma_{k-z})$ in (17).

The ability to predict noise implies an ability to predict detection limits. The first step is to estimate the photon-counting rates associated with an arbitrary scattering coefficient. Given calibration constants, K_2, K_4, W, and W_b, (4) and (5) may be solved for the normalized photon-counting rates, C_m and C_{mb}, respectively. Scaled counting rates may then be estimated by assuming $C_{s-\text{dark}}$ and $C_{s-\text{cal}}$ are constant and solving (24) for $C_{s-\text{sig}}$. Given an averaging time τ, the scaled counting rates may be converted to an estimated noise level via (27) and (28). Calculating noise in this manner and defining detection limits as a signal-to-noise ratio of 2, detection limits as a function of averaging time are shown in Table 4.

Photon-counting uncertainty affects the accuracy of the gas calibration and zeroing procedures. This source of error (which introduces systematic error for measurements based on one calibration but random error for long-term averages based on a large number of calibrations) may be estimated given the averaging time used during calibrations (300 s in our case) and assuming that errors due to incomplete flushing of the sensing volume prior to calibration are negligible. Uncertainties in photon counts during calibration and zeroing con-

TABLE 4. Detection limits* (Mm^{-1}) as a function of averaging time.

	Averaging time (s)					
	2	10	60	300	1800	9000
(a) Measurement photon-counting noise only						
σ_{sp}^{450}	3.76	1.62	0.65	0.29	0.12	0.05
σ_{sp}^{550}	1.40	0.61	0.25	0.11	0.05	0.02
σ_{sp}^{700}	2.18	0.95	0.38	0.17	0.07	0.03
σ_{bsp}^{450}	2.56	1.09	0.43	0.19	0.08	0.04
σ_{bsp}^{550}	0.93	0.40	0.16	0.07	0.03	0.01
σ_{bsp}^{700}	1.82	0.79	0.32	0.14	0.06	0.03
(b) Measurement noise plus noise during zeroing procedure**						
σ_{sp}^{450}	3.95	1.86	0.85	0.44	0.38	0.33
σ_{sp}^{550}	1.47	0.70	0.33	0.17	0.14	0.13
σ_{sp}^{700}	2.29	1.09	0.49	0.26	0.22	0.20
σ_{bsp}^{450}	2.69	1.25	0.56	0.29	0.25	0.22
σ_{bsp}^{550}	0.98	0.46	0.21	0.11	0.09	0.08
σ_{bsp}^{700}	1.91	0.91	0.42	0.21	0.18	0.16

* Defined by signal-to-noise ratio of 2, where noise is predicted photon-counting uncertainty.
** Assuming a fixed averaging time for the zeroing procedure of 300 s.

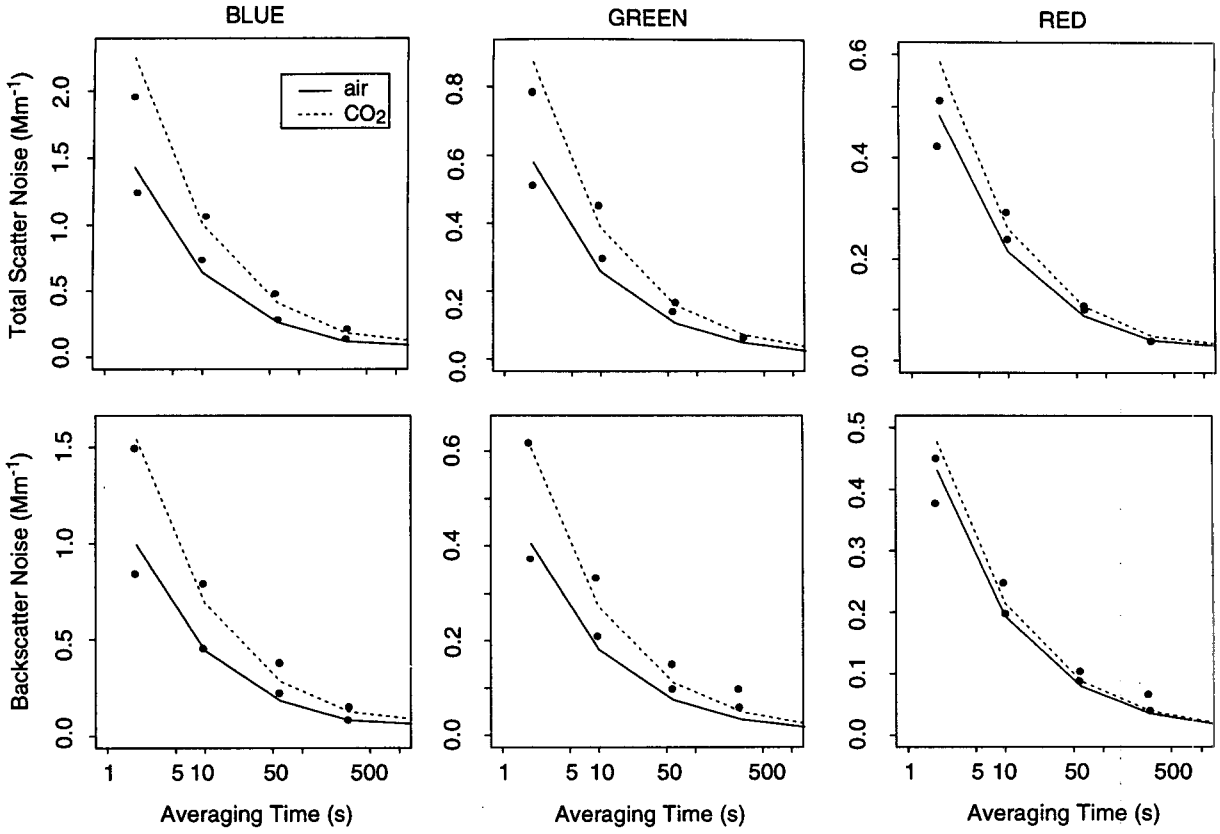

FIG. 5. Predicted (lines) and measured (points) nephelometer noise. As described in the text, the prediction is based on photon-counting statistics and the measurement on the standard deviation of repeated measurements under steady conditions.

tribute to measurement uncertainty via the terms $\delta(C_{hi} - C_{lo})$ and $\delta(C_m - C_z)$, respectively, as shown in (17).

Are there other sources of random error that contribute significantly to calibration uncertainty? To answer this question, noise-induced uncertainty in the calibration constants was calculated by applying the general uncertainty equation, (14), to (10)–(13). These calculated uncertainties were then compared to measured uncertainties based on repeated calibrations (10 each) and zeroings (16 each). Measured uncertainty was assessed as the standard deviation of the K_2, K_4, W, and W_b values determined by these repeated procedures. The predicted and measured uncertainties are compared in Table 5. Considering the small sample sizes, the agreement is very good (well within a factor of 2). Most importantly, there is no evidence that predicted uncertainty, based only on photon-counting uncertainty, is an underestimate. As in the case of measurement noise, this implies that photon-counting statistics are the only significant source of random error affecting the calibration and zeroing procedures.

Equation (17) shows how photon-counting uncertainties combine with uncertainties in the calibration gas scattering coefficients to yield a total measurement uncertainty (neglecting nephelometer nonidealities). Three separate contributing terms are indicated in (17), but the calibration gas (σ_k) uncertainties actually divide into literature and environmental (gas density) uncertainties, as discussed in relation to (18) and (19). Thus, there are four logically separable contributing terms. These are compared and summed in Table 6 for two levels of particle scattering. Table 6a indicates that calibration errors approach zero as particle scattering levels approach zero. In this case, uncertainty is completely dominated by measurement noise and noise during the zeroing procedure. Table 6b shows that at higher particle scattering levels, the dominant source of uncertainty for 60-s averaging is uncertainty in the literature values of air and CO_2 scattering coefficients. In section 4 we will consider the implications of these comparisons.

It is important to note that the photon-counting rates for a fixed scattering value (e.g., those presented in Table 3) are highly variable. This variability is due to 1) unit-to-unit differences especially in photomultiplier tube (PMT) sensitivity, 2) drift over time, and 3) user-controllable lamp power and PMT voltages. Thus, while the counting uncertainties presented here are typical, they are not a fixed feature of the model 3563 nephelometer. What is important is the ability to predict

TABLE 5. Calibration uncertainty due to photon-counting uncertainty.

	Pred	Meas	Meas/pred
δK_2 (m^{-1}) × 1000			
Blue	0.024	0.032	1.33
Green	0.021	0.019	0.90
Red	0.042	0.070	1.67
δK_4 × 100			
Blue	0.470	0.770	1.64
Green	0.430	0.380	0.88
Red	0.950	1.060	1.12
δW (m^{-1}) × 10^6			
Blue	0.118	0.096	0.82
Green	0.047	0.043	0.91
Red	0.040	0.044	1.10
δW_b (m^{-1}) × 10^6			
Blue	0.082	0.057	0.69
Green	0.033	0.026	0.80
Red	0.036	0.029	0.82

Abbreviations: pred — predicton; meas — measurement.

noise levels from reported photon-counting rates. Because of this ability, signal-to-noise ratios can be assessed accurately and it is possible to optimize calibration procedures, lamp power, and PMT voltages for a given application.

b. *Gas tests 2: Linearity of response*

Following the standard two-point calibration described earlier (Fig. 2), accurate nephelometer measurements require a linear response to varying scattering coefficient. A straightforward test of this linearity is to measure the nephelometer response to a particle-free gas of varying density. We performed this test by varying gas number density in eight discrete steps from 0.2 to 0.8 of STP (0°C, 1013.2 mb). Tests with two nephelometers, two gases (air and HFC134a), and three wavelengths for both total scatter and backscatter constitute 24 linearity tests with 192 data pairs of scattering coefficient and gas density. The range of scattering coefficients is from 0.2 to about 6 times the Rayleigh scattering of air at STP. Of the 24 tests, 22 yielded linear regression correlation coefficients r^2 larger than 0.999, while the remaining two (both in red) yielded r^2 values larger than 0.990. This indicates a highly linear response over a broad range of scattering coefficients. In addition, these tests demonstrate an absence of significant mechanical deformation affecting the measurements when the instrument is operated at pressures down to 200 mb.

c. *Particle tests*

Tests with nearly monodisperse DES particles were used to assess how well the TSI 3563 nephelometer measurements of $\sigma^{\lambda_i}{}_{sp}$ and $\sigma^{\lambda_i}{}_{bsp}$ can be predicted from Mie theory when (a) tests are conducted on laboratory particles that satisfy the Mie assumptions and (b) the measured wavelength and angular sensitivities of the nephelometer are taken into account. This constitutes a closure experiment as shown in Fig. 3b. If the discrepancies between the actual nephelometer measurement

TABLE 6. Nephelometer uncertainties due to noise and calibration.

	Meas. and zero photon counts	Calibration photon counts	Calib. gases, environment	Calib. gases, literature	Sum
(a) Particle scattering = 0					
$\delta\sigma_{sp}^{450}$	0.28	0.00	0.00	0.00	0.28
$\delta\sigma_{sp}^{550}$	0.11	0.00	0.00	0.00	0.11
$\delta\sigma_{sp}^{700}$	0.10	0.00	0.00	0.00	0.10
$\delta\sigma_{bsp}^{450}$	0.20	0.00	0.00	0.00	0.20
$\delta\sigma_{bsp}^{550}$	0.08	0.00	0.00	0.00	0.08
$\delta\sigma_{bsp}^{700}$	0.09	0.00	0.00	0.00	0.09
(b) Particle scattering = 1.6 × (air scattering)					
$\delta\sigma_{sp}^{450}$	0.42	0.22	0.23	0.56	0.77
$\delta\sigma_{sp}^{550}$	0.16	0.08	0.10	0.25	0.32
$\delta\sigma_{sp}^{700}$	0.11	0.06	0.04	0.09	0.16
$\delta\sigma_{bsp}^{450}$	0.29	0.10	0.11	0.27	0.43
$\delta\sigma_{bsp}^{550}$	0.11	0.04	0.05	0.12	0.18
$\delta\sigma_{bsp}^{700}$	0.09	0.03	0.02	0.05	0.11

Evaluation of terms in Eq. (17) for two different levels of particle scattering corresponding to (a) zero and (b) 1.6 times $\delta_{k-\text{air}}$ at 293 K and 950 mb [see Table 1 and Eq. (18)]. The term in (17) labeled "calibration gases" has been split into environmental (T, P) uncertainties and literature (STP) uncertainties, as discussed in the text. Photon count uncertainties were evaluated using the counting rates from Table 3 with averaging times of 300, 300, and 60 s for calibration, zeroing, and measurements, respectively. Calibration gas uncertainties are given in Table 1 and Eq. (21). Sum—square root of the sum of the squares of the previous four columns. All values shown are absolute uncertainties (Mm^{-1}).

σ_m and the independently predicted nephelometer measurement σ_p are within experimental uncertainties, then the theoretical and experimental methods are validated and their combined uncertainty is established.

Tests were conducted at four sizes (central diameters, D_{pc}, of 0.2, 0.4, 0.5, and 0.6 μm), spanning most of the accumulation mode size range. At one size (D_{pc} = 0.4 μm), concentration was varied by changing the dilution flow such that a total of six independent tests were performed. In Fig. 6, both σ_m and σ_p have been normalized by the measured particle number concentration, N (cm^{-3}), in order to display the results as a function of particle diameter. Predicted scattering and backscattering are plotted as continuous lines, while measured values are plotted as points.

Table 7a summarizes the conditions for each test and Table 7b evaluates closure in relation to both the average and the maximum discrepancies among the tests. Experimental uncertainty was estimated as the sum of contributions from nephelometer noise and calibration uncertainty [using Eq. (17)] and from uncertainties in generating and counting the DES particles [using the stated uncertainties in each contributing term and Eqs. (14) and (35)]. Because uncertainties are estimated as the quadratic sum of the various contributing terms (i.e., implicitly assuming no correlation among terms), they are likely to underestimate the maximum uncertainty associated with individual tests. Table 7b shows that discrepancies for all parameters are within experimental uncertainty when average discrepancies are compared to average experimental uncertainties and maximum discrepancies are compared to twice the experimental uncertainty for the corresponding test.

Overall, this indicates a successful closure experiment and an objective determination that the TSI 3563 nephelometer measurements for accumulation mode particles can be predicted by Mie theory with an average uncertainty of at most 10%. Table 6 also shows that the experimental uncertainties for these tests are dominated by particle generation uncertainties, not nephelometer uncertainties. Therefore, it is possible that improved experimental procedures could demonstrate even better agreement.

d. Evaluation of nephelometer size-dependent performance

As shown in Fig. 3b, calculation of σ_p incorporates the wavelength and angular sensitivities of the nephelometer into a modified Mie integral. The previous section established that σ_p is indeed a good predictor of the actual nephelometer measurement σ_m. In this sec-

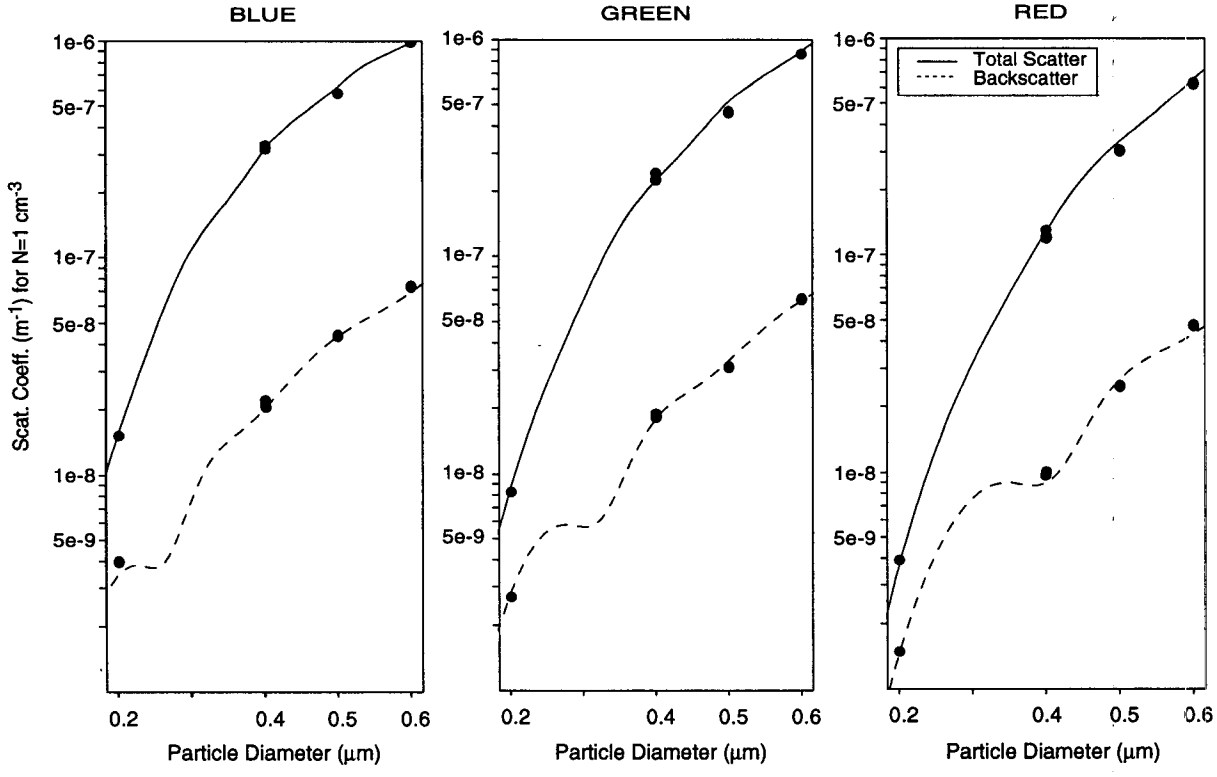

FIG. 6. Aerosol particle tests with varying particle size. Comparison of predicted (lines) and actual (points) nephelometer measurements normalized by particle number concentration in air N. As described in the text, the predicted measurement incorporates nephelometer wavelength and angular nonidealities. Quantitative discrepancies are summarized and compared to experimental uncertainties in Table 7.

TABLE 7. Closure experiments with nearly monodisperse particles.

(a) Test conditions

Test	D_{pc} (μm)	W	N (cm^{-3})	τ (s)	σ_{sp}^{550} (Mm^{-1})	σ_{bsp}^{550} (Mm^{-1})
1	0.200	0.20	1477	1560	12	3.9
2	0.400	0.20	116	240	27	2.1
3	0.400	0.20	226	480	50	4.0
4	0.400	0.20	291	180	66	5.3
5	0.500	0.20	707	1080	324	22
6	0.600	0.20	545	3060	464	34
Uncertainty	±2%	±0.04	±1%			

(b) Closure analysis

	Total scatter			Backscatter		
	Blue	Green	Red	Blue	Green	Red
Ave. discrep.	−4.7%	−4.6%	−2.9%	−0.3%	−2.3%	6.1%
Ave. abs. discrep.	4.7%	5.1%	4.4%	3.8%	4.1%	7.2%
Ave. exp. uncert.	±7.6%	±7.8%	±10.1%	±7.5%	±7.9%	±8.1%
Ave. gen. uncert.	±7.3%	±7.6%	±9.8%	±6.6%	±7.6%	±6.7%
Ave. neph. uncert.	±1.8%	±1.7%	±2.4%	±3.4%	±2.2%	±4.0%
Max. discrep. test No.	5	5	5	1	5	2
Max. discrep.	−11%	−13%	−9%	9%	−10%	11%
2 × (exp. uncert.)	13%	15%	15%	9%	16%	18%

D_{pc} and W are the central diameter and relative width of the triangular size distribution transmitted by the differential mobility analyzer; N is the particle number concentration measured within the nephelometer; τ is the sample time for the nephelometer measurement; σ_{sp}^{550} and σ_{bsp}^{550} are the measured scattering coefficients measured at 550-nm wavelength. Uncertainty values given at the bottom of part (a) were used in the calculation of $\delta\sigma_p$: ave. discrep. — average of $(\sigma_m - \sigma_p)/\sigma_p$; ave. abs. discrep. — average of $|\sigma_m - \sigma_p|/\sigma_p$; ave. exp. uncert. — average of $(\delta\sigma_m^2 + \delta\sigma_p^2)^{-1/2}/\sigma_p$; ave. gen. uncert. — average of $\delta\sigma_p/\sigma_p$, where $\delta\sigma_p$ is the portion of experimental uncertainty due to the generation and counting of particles of known size distribution and refractive index; ave. neph. uncert. — average of $\delta\sigma_m/\sigma_p$, where $\delta\sigma_m$ is the portion of experimental uncertainty due to nephelometer noise and calibration uncertainties as summarized in Eq. (17); max. discrep. test # — test number that produced the maximum value of $|\sigma_m - \sigma_p|/\sigma_p$; max. dscrep. — $(\sigma_m - \sigma_p)/\sigma_p$ for the max. discrep. test; 2 × (exp. uncert.) — twice the experimental uncertainty for the max. discrep. test.

tion, we evaluate the effects of nephelometer nonidealities by comparing σ_p to the true scattering or backscattering coefficient σ_k. Because both σ_p and σ_k are calculated quantities, the comparison can be made for arbitrary size distributions and refractive indices.

Figure 7 illustrates the size-dependent nephelometer performance for lognormal size distributions, assuming a refractive index of $(1.45 - 0i)$ and geometric standard deviation of 2. Note that the predicted nephelometer error is less than 20% for all values of geometric volume mean diameter D_{gv} less than 1 μm. For typical accumulation-mode size distributions ($0.2 < D_{gv} < 0.4$), errors are less than 10%. Note also that errors for backscatter and total scatter are in the opposite sense for accumulation mode particles where nephelometer nonidealities will result in a systematic exaggeration of the backscatter-to-total-scatter ratio R by up to about 15%. For coarse-mode particles ($D_{gv} > 1$ μm) nephelometer errors remain modest for backscatter (<10%) but increase dramatically for total scatter (20%–50%). This reflects the fact that for large particles, σ_{sp} becomes increasingly dominated by scattering in the near-forward direction where it is not sensed by the nephelometer. Note that measurements of R on coarse mode particles will be exaggerated by nearly the same relative amount that total scattering is underestimated.

4. Discussion

a. *Sources of uncertainty*

For low concentrations and/or short sampling times, photon-counting statistics tend to dominate nephelometer uncertainty. We have shown that this portion of uncertainty can be assessed accurately from the photon-counting rates reported by the TSI 3563 nephelometer. While detection limit has been defined in the past with regard to noise during the air-plus-particle measurement (e.g., Bodhaine et al. 1991), noise during the filtered-air measurement (i.e., during the zeroing procedure) must be considered as well, since the derived particle scattering coefficient depends on the quantity $(C_m - C_z)$, as shown in (17). The two definitions of detection limit are compared in Table 4 for a fixed filtered-air averaging time of 300 s. As shown in Table

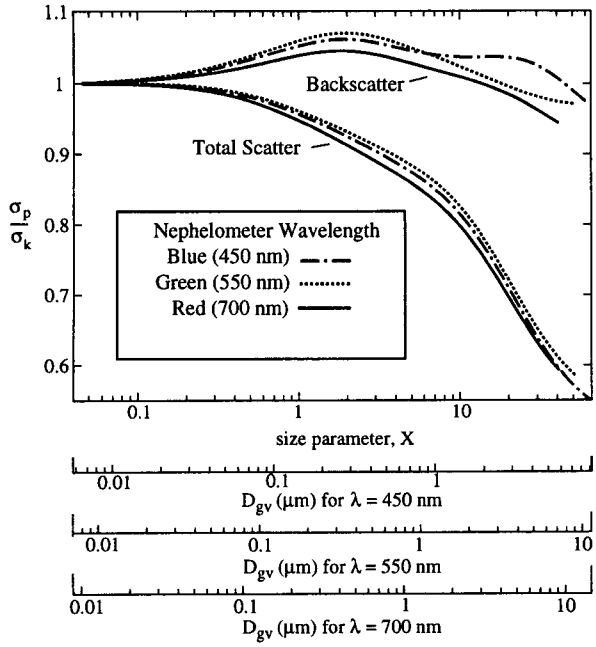

FIG. 7. Predicted nephelometer performance for lognormal distributions. For a given volume mean diameter D_{gv}, the known scattering coefficient σ_k is calculated from standard Mie theory, and the predicted nephelometer measurement σ_p is calculated from a modified Mie integration that incorporates the nephelometer wavelength and angular nonidealities. Assumed values for the particle refractive index and the geometric standard deviation of the size distribution are 1.45 and 2, respectively. The ratio of σ_p to σ_k is plotted for total scatter and backscatter at each of the three nephelometer wavelengths. The primary x axis is size parameter $X = \pi D_{gv}/\lambda$. Additional x axes show the particle diameters for each wavelength. The small differences among the wavelengths for the same size parameter are due to different wavelength sensitivities (Fig. 4a).

4b, increasing the averaging time for the air-plus-particle measurement much beyond the averaging time for the filtered-air measurement will not produce a significant decrease in detection limit. This implies that for measurements near the detection limit, the optimal strategy would be to devote approximately equal time to filtered-air and air-plus-particle measurements. While the detection limits reported in Table 4 are somewhat higher than those reported by previous investigators for similar designs (Heintzenberg and Bäcklin 1983; Bodhaine et al. 1991), this does not imply poorer performance by the TSI 3563 but rather a more rigorous definition and determination procedure. We can state this with confidence because the photon-counting rates of the TSI 3563 are very similar to those reported by Bodhaine et al. (1991) and we have shown that there are no significant sources of random uncertainty other than photon-counting statistics.

For particle scattering coefficients above about 1 Mm^{-1} and averaging times longer than about 60 s, systematic rather than random sources of uncertainty become dominant. Systematic uncertainties logically divide into uncertainties associated with the gas calibration, which are not size-dependent and that are assessed in Table 6, and uncertainties due to wavelength and angular nonidealities, which are strongly size dependent, as shown in Fig. 7. Calibration uncertainties divide into photon-counting uncertainties during the calibration, gas density uncertainties during the calibration, and uncertainties in the literature values of the calibration gas scattering coefficients at STP. Together, calibration uncertainties introduce about a 1% uncertainty to particle scattering measurements, which is small compared to uncertainties associated with nephelometer nonidealities. Moreover, calibration uncertainties are dominated by uncertainty in the scattering coefficient of the high span gas, CO_2, at STP, $\sigma_{k-CO_2}(\text{STP})$, which is not a function of nephelometer performance. Thus, improvements in the temperature and pressure measurements (which would reduce gas density uncertainties) and/or increases in calibration averaging times much beyond the 300 s used here (which would reduce photon-counting uncertainties during calibration) are not warranted at this time. On the other hand, the TSI nephelometer itself offers an excellent tool for reducing uncertainty in $\sigma_{k-CO_2}(\text{STP})$ as discussed in section 4c.

The gas calibration procedure corrects for nephelometer nonidealities in the small particle limit, but this Rayleigh-regime correction becomes imperfect in the Mie scattering regime due to changes in the distribution of scattered light. The dominant nephelometer nonideality is the forward scattering truncation from 0° to approximately 7°. Because particle scattering becomes increasingly concentrated into the forward lobe as particle size increases, forward truncation errors are always negative (i.e., σ_{sp} is underestimated) and increase systematically with particle size. This source of error, which is the dominant feature in Fig. 7, is modest (a few to 10%) for accumulation mode (submicrometer) particles but rather severe (20%–50%) for coarse mode (supermicrometer) particles. In contrast, nephelometer measurements of σ_{bsp} remain quite accurate (well within ±10%) up to particle diameters of at least 10 μm. Errors arising from wavelength nonidealities are responsible for the differences among the three backscatter and the three total scatter curves in Fig. 7. These errors are of order 2%–3% and do not vary systematically with size.

The issue of water vapor affecting σ_{k-air} should be carefully considered for high-RH or varying-RH measurements for which σ_{sp} or σ_{bsp} is less than σ_{k-air}. For instance, (23) and the text immediately following indicate that at 30°C operating temperature, σ_{k-air} will decrease by 0.7% between 30% and 85% RH. Thus, if dual-RH measurements were made on a completely hydrophobic aerosol with a scattering level σ_{sp} that was 10% of σ_{k-air}, there would be an apparent (erroneous) 7.2% decrease in σ_{sp} in changing RH from 30% to 85%. Because this effect varies inversely with the absolute

magnitude of σ_{sp}, it will generally be greater at longer wavelengths and for σ_{bsp}.

b. *Nephelometer applications*

Based on our investigation of the performance characteristics of the TSI 3563 nephelometer, we suggest the following general areas of application:

1) Measuring the scattering coefficient of arbitrary gases. Accuracy here is limited only by the nephelometer calibration and photon-counting statistics. Uncertainties within ±1% can be achieved.

2) Measuring the scattering coefficient of submicrometer particles. Accuracy is reduced by nephelometer nonidealities but is still quite good (generally well within ±10%). Removal of supermicron particles by impaction ahead of the nephelometer is required to achieve this accuracy. Importantly, the accuracy is not affected by the composition or physical state of the particles.

3) Use the six measured parameters to derive intensive optical properties of submicrometer particles. The backscatter-to-total-scatter ratio and the wavelength dependence of particle scattering can be measured by the 3563 nephelometer to well within ±20%. For accumulation mode particles, there is a small but systematic tendency to overestimate the backscatter-to-total-scatter ratio. Independent measurements of particulate mass and chemical composition allow other intensive properties—for example, mass scattering efficiency or component scattering efficiency—to be derived.

4) Use humidity preconditioning of the sampled aerosol to study how particulate scattering is affected by hydration.

For these experiments, additional sources of uncertainty (not discussed here) include the accuracy of RH control, the variations of RH within the nephelometer due to sample heating by the lamp, and possible kinetic effects preventing particles from achieving equilibrium levels of hydration. Taken together, applications 2, 3, and 4 allow a determination of the key aerosol properties relative to their radiative/climatic effects.

c. *Future work*

The main source of calibration uncertainty is uncertainty in the scattering coefficient of CO_2 (and the other potential high-span gases.) Laboratory studies to reduce this uncertainty could be carried out with a 3563 nephelometer calibrated with air and He or with air at two densities. Reducing the uncertainty of $\sigma_{k-\mathrm{hi}}(\mathrm{STP})$ for calibration gases CO_2, SF_6, and HFC-134a to the uncertainty of $\sigma_{k-\mathrm{air}}(\mathrm{STP})$ would be extremely useful. In addition, careful measurements of the water vapor effect on $\sigma_{k-\mathrm{air}}$, estimated in (23), would be useful for RH-scanning nephelometer.

While the particle tests described herein did find agreement within experimental uncertainty, these tests could be made more rigorous by 1) reducing the experimental uncertainty (especially the uncertainties of particle size and concentration) and 2) conducting tests at larger (i.e., supermicron) particle sizes where the effects of nephelometer nonidealities are predicted to be much greater. The difficulty of producing and conveying known concentrations of large particles prevented their inclusion in this work.

5. Conclusions

The performance characteristics of a high-sensitivity, three-wavelength, total scatter/backscatter nephelometer (TSI, Inc., model 3563) have been investigated through laboratory experiments with gases of known scattering coefficient and particles of known size and refractive index. The overall goal is to understand uncertainties associated with the nephelometer measurement of light scattering and hemispheric backscattering by particles. Key results are as follows:

- Nephelometer measurements rely on calibration with gases of known scattering coefficient and an assumption of linear response to varying scattering coefficient. Tests with gases of varying refractive index and density (down to 0.2 atm) showed that the linearity assumption is extremely reliable.
- For low particle concentrations or short sampling times, random noise is the dominant source of nephelometer uncertainty. For typical operating conditions and a signal-to-noise criterion of 2, the detection limits for 5-min averages are 0.2 and 0.1 Mm^{-1} for total scatter and backscatter, respectively, at 550 nm. This assessment includes noise during the zeroing procedure with filtered air.
- Noise levels for arbitrary conditions can be predicted accurately from the photon counts during the gas calibration procedure, which are reported by the 3563 nephelometer. Thus, noise levels and detection limits for each instrument and application can be determined and, to a large extent, controlled by adjustments to lamp brightness, measurement sample times, and the frequency and duration of filtered-air measurements.
- For particle scattering coefficients above about 1 Mm^{-1} and averaging times longer than about 60 s, systematic rather than random sources of uncertainty become dominant. These logically divide into gas-calibration uncertainties, which are independent of particle size, and uncertainties due to wavelength and angular nonidealities, which are strongly size dependent.
- The gas calibration contributes about a ±1% uncertainty to particle scattering measurements. The dominant cause is uncertainty in the scattering coefficient of the high span gas CO_2. (Other potential span gases are even less accurately known.) Reduction of this uncertainty would be useful and could be undertaken with

a 3563 nephelometer calibrated with air and He or with air at two densities.

• A larger source of systematic uncertainty stems from nonidealities in the wavelength and angular sensitivities of the 3563 nephelometer. These nonidealities (which are a feature of any practical nephelometer design) were measured and incorporated into a theoretical nephelometer simulation. Using nearly monodisperse, laboratory particles of known size, refractive index, and number concentration, predicted and actual nephelometer measurements were found to agree within experimental uncertainties of ±10%. This *closure* experiment provides an objective measure of the combined uncertainties associated with the nephelometer integration of light scattering by particles, the generation of particles of known optical properties, and the modified Mie integration used to simulate the nephelometer. Because experimental uncertainty for these tests was dominated by particle generation uncertainty, future laboratory experiments may be able to demonstrate even better closure.

• Extrapolating our nephelometer simulation to the continuum of particle sizes, we find that nephelometer nonidealities introduce uncertainties of less than 10% for typical accumulation mode particles sizes (i.e., volume mean diameters between 0.2 and 0.4 μm). For coarse mode particles (diameters greater than 1 μm) nephelometer errors remain modest for backscatter (<10%) but increase dramatically for total scatter (20%–50%). This reflects the fact that the nephelometer does not sense near-forward scattering, which becomes an increasing dominant part of total scattering for large particles.

• Based on these findings, the 3563 nephelometer appears highly suited for at least four types of applications: 1) measuring the scattering coefficients of arbitrary gases, 2) measuring the scattering coefficients of accumulation mode particles (which requires removal of coarse mode particles by impaction), 3) using the six measured scattering coefficients to derive aerosol optical properties such as the backscatter-to-total-scatter ratio and the wavelength dependence of light scattering, and 4) using humidity preconditioning of the sampled aerosol to study how light scattering is affected by particle hydration. Taken together, applications 2, 3, and 4 allow a determination of key aerosol properties relative to their radiative/climatic effects.

Acknowledgments. This work was supported by the National Science Foundation (Grant ATM-9311213) and the National Oceanic and Atmospheric Administration (JISAO Cooperative Agreement NA37RJ0198, Contribution number 346). Facilities for the experiments were provided by TSI, Inc., St. Paul, Minnesota.

APPENDIX

Angular Integration by an Ideal Nephelometer

During its passage through the atmosphere, light is attenuated according to the Beer–Lambert law,

$$\frac{dI}{I} = -\sigma_{\text{ext}} dz, \tag{A1}$$

where dz is an increment of distance and σ_{ext}, the volume extinction coefficient (m^{-1}), consists of four separable components due to scattering and absorption by particles and gases. The particulate scattering coefficient σ_{sp} and hemispheric backscatter coefficient σ_{bsp} for a given wavelength λ can be expressed as the integral over scattering angle θ of the particulate volume scattering function $\beta_p(\theta)$ (m^{-1} sr^{-1}) (Middleton 1952, 16–17):

$$\sigma_{sp} = 2\pi \int_0^{\pi} \beta_p(\theta) \sin\theta d\theta \tag{A2a}$$

$$\sigma_{bsp} = 2\pi \int_{\pi/2}^{\pi} \beta_p(\theta) \sin\theta d\theta, \tag{A2b}$$

where $\beta_p(\theta)$, in turn, can be related to scattering by a population of particles with number concentration N and size distribution $N(D)$ by

$$\beta_p(\theta) = \int_0^{\infty} \frac{|S(\theta, X, m)|^2}{2\pi X^2} \frac{\pi D^2}{4} \frac{\partial N}{\partial \log D} d\log D, \tag{A3}$$

where $|S(\theta, X, m)|^2$ is the scattering intensity function for a single particle of size parameter X ($=\pi D\lambda^{-1}$) and complex refractive index m. For an internally homogeneous sphere, the dependence of S on θ, X, and m is described by Mie theory.

Scattered light sensed by the nephelometer represents a geometrical integration of $\beta_p(\theta)$ such that, in the ideal case, its signal is proportional to σ_{sp} and σ_{bsp}. This geometrical integration will now be derived.

Here $\beta_p(\theta)$ is the proportionality constant relating incident flux density F_{dv} (W m^{-2}) impinging on a volume element dv (m^3) to scattered intensity $I(\theta)$ (W sr^{-1}):

$$I(\theta) = F_{dv}\beta_p(\theta)dv. \tag{A4}$$

Within the nephelometer, cylindrical volume elements correspond to each scattering angle θ as shown in Fig. A1. The illumination flux density along the nephelometer axis is given by

$$F_{dv} = \frac{\text{power}}{\text{area}} = \frac{I_0\omega_\phi}{h^2\omega_\phi \sec\phi} = \frac{I_0 \cos\phi}{h^2}, \tag{A5}$$

where I_0 is the illumination intensity constant for an isotropic (Lambertian) emitter, ϕ is the illumination angle with respect to the nephelometer axis, ω_ϕ is the increment of solid angle represented by dv with respect to the light source, and both the volume element and the light source are assumed to be points. Using the geometrical relations $\sin\theta = \cos\phi$ and $h = y \csc\theta$, we have

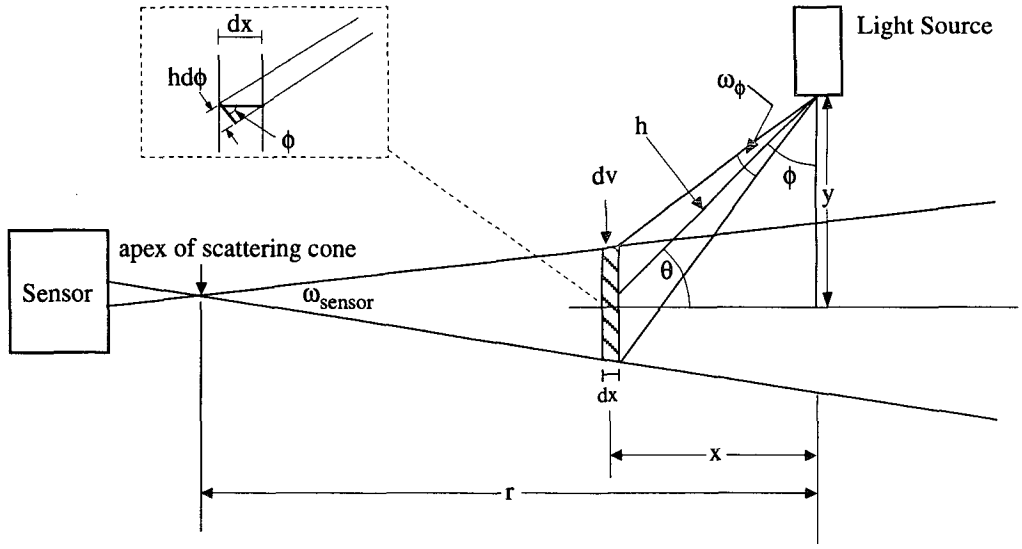

FIG. A1. Nephelometer geometry used in deriving the angular integration of scattering. The vertical scale is greatly exaggerated.

$$F_{dv} = \frac{I_0 \sin\theta}{y^2 \csc^2\theta} = \frac{I_0 \sin^3\theta}{y^2}. \quad \text{(A6)}$$

The volume of each cylindrical scattering element is dx times the disc area. For small increments, $dx = h \sec\phi d\phi = h \csc\theta d\theta$ and for small values of ω_{sensor} the disc area is $(r - x)^2\omega_{\text{sensor}}$. Using these relations (and $h = y \csc\theta$ from above),

$$dv = (r - x)^2\omega_{\text{sensor}} y \csc^2\theta d\theta. \quad \text{(A7)}$$

Equation (A4) may now be rewritten as

$$I(\theta) = \frac{I_0}{y}(r - x)^2\omega_{\text{sensor}}\beta_p(\theta)\sin\theta d\theta. \quad \text{(A8)}$$

Considering the volume element dv to be a point source of scattered light with intensity distribution described by (A8), the increment of flux density received at the sensor dF_{sensor} will be inversely related to the square of the distance to the sensor:

$$dF_{\text{sensor}} = \frac{I(\theta)}{(r - x)^2}. \quad \text{(A9)}$$

Substituting from (A8) into (A9) and integrating over all volume elements (that is, over all scattering angles),

$$F_{\text{sensor}} = K\int \beta_p(\theta)\sin\theta d\theta, \quad \text{(A10)}$$

where $K\ (= I_0\omega_{\text{sensor}}/y)$ is an instrumental constant.

Comparing (A2) and (A10) shows that the nephelometer signal for this idealized case will be proportional to σ_{sp} and σ_{bsp} given the same limits of integration. The key assumptions for this geometrical derivation are that the nephelometer senses scattering from 0° to 180° for total scatter and 90° to 180° for backscatter, that each volume element acts as a point source of scattered light, and that the sensing volume is illuminated by a point source of isotropic light. An additional (nongeometric) assumption for the measurement of $\sigma^{\lambda_i}{}_{sp}$ and $\sigma^{\lambda_i}{}_{bsp}$, where λ_i represents one of the nominal nephelometer wavelengths, is that the nephelometer responds to monochromatic radiation at the exact nominal wavelength. How practical nephelometer designs differ from this idealized case is discussed in the main text along with the consequences of these differences.

REFERENCES

Ahlquist, N. C., and R. J. Charlson, 1967: A new instrument for evaluating the visual quality of air. *J. Air Pollut. Control Assoc.*, **17,** 467–469.

Alms, G. R., A. K. Burnham, and W. H. Flygare, 1975: Measurement of the dispersion in polarizability anisotropies. *J. Chem. Phys.*, **63,** 3321–3326.

Beuttell, R. G., and A. W. Brewer, 1949: Instruments for the measurement of visual range. *J. Sci. Instrum. Phys. Ind.*, **26,** 357–359.

Bhardwaja, P. S., R. J. Charlson, A. P. Waggoner, and N. C. Ahlquist, 1973: Rayleigh scattering coefficients of Freon-12, Freon-22, and CO2 relative to that of air. *Appl. Opt.*, **12,** 135.

Bodhaine, B. A., N. C. Ahlquist, and R. C. Schnell, 1991: Three-wavelength nephelometer suitable for aircraft measurements of background aerosol scattering extinction coefficient. *Atmos. Environ.*, **25A,** 2267–2276.

Bucholtz, A., 1995: Rayleigh-scattering calculations for the terrestrial atmosphere. *Appl. Opt.*, **34,** 2765–2773.

Charlson, R. J., W. M. Porch, A. P. Waggoner, and N. C. Ahlquist, 1974: Background aerosol light scattering characteristics: nephelometric observations at Mauna Loa Observatory compared with results at other remote locations. *Tellus,* **26,** 345–360.

Covert, D. S., R. J. Charlson, and N. C. Ahlquist, 1972: A study of the relationship of chemical composition and humidity to light scattering by aerosols. *J. Appl. Meteor.*, **11,** 968–976.

CRC, 1994: *Handbook of Chemistry and Physics.* 75th ed. Chemical Rubber Co., 2348 pp.

Cutten, D. R., 1974: Rayleigh scattering coefficients for dry air, carbon dioxide, and freon-12. *Appl. Opt.*, **13,** 468–469.

Eldén, B., 1966: The refractive index of air. *Metrologia,* **2,** 71–80.

Ensor, D. S., and A. P. Waggoner, 1970: Angular truncation error in the integrating nephelometer. *Atmos. Environ.,* **4,** 481–487.

——, and P. S. Bhardwaja, 1976: On the accuracy of the backward hemispheric integrating nephelometer. *J. Appl. Meteor.,* **15,** 1092–1096.

Heintzenberg, J., 1978: The angular calibration of the total scatter/backscatter nephelometer, consequences and applications. *Staub–Reinhalt. Luft,* **38,** 62–63.

——, and L. Bäcklin, 1983: A high sensitivity integrating nephelometer for airborne air pollution studies. *Atmos. Environ.,* **17,** 433–436.

King, L. V., 1923: On the complex anisotropic molecule in relation to the dispersion and scattering of light. *Proc. Roy. Soc. London, Ser. A,* **104,** 333–357.

Kinney, P. D., D. Y. H. Pui, G. W. Mulholland, and N. P. Bryner, 1991: Use of the electrostatic classification method to size 0.1 μm SRM particles—A feasibility study. *J. Res. Natl. Inst. Stand. Technol.,* **96,** 147–176.

Merck, 1989: *The Merck Index.* Merck & Co., 1606 pp.

Middleton, W. E. K., 1952: *Vision Through the Atmosphere.* University of Toronto Press, 250 pp.

Owens, J. C., 1967: Optical refractive index of air: dependence on pressure, temperature and composition. *Appl. Opt.,* **6,** 51–59.

Penndorf, R., 1957: Tables of the refractive index for standard air and the Rayleigh scattering coefficient for the spectral region between 0.2 and 20 μm and their application to atmospheric optics. *J. Opt. Soc. Amer.,* **47,** 176–182.

Young, A. T., 1980: Revised depolarization corrections for atmospheric extinction. *Appl. Opt.,* **19,** 3427–3428.